FULL PAPER

Vertically Segregated Structure and Properties of Small Molecule–Polymer Blend Semiconductors for Organic Thin-Film Transistors

Nayool Shin, Jihoon Kang, Lee J. Richter, Vivek M. Prabhu, R. Joseph Kline, Daniel A. Fischer, Dean M. DeLongchamp, Michael F. Toney, Sushil K. Satija, David J. Gundlach, Balaji Purushothaman, John E. Anthony, and Do Y. Yoon**

A comprehensive structure and performance study of thin blend films of the small-molecule semiconductor, 2,8-difluoro-5,11-bis(triethylsilylethynyl) anthradithiophene (diF-TESADT), with various insulating binder polymers in organic thin-film transistors is reported. The vertically segregated composition profile and nanostructure in the blend films are characterized by a combination of complementary experimental methods including grazing incidence X-ray diffraction, neutron reflectivity, variable angle spectroscopic ellipsometry, and near edge X-ray absorption fine structure spectroscopy. Three polymer binders are considered: atactic poly(α-methylstyrene), atactic poly(methylmethacrylate), and syndiotactic polystyrene. The choice of polymer can strongly affect the vertical composition profile and the extent of crystalline order in blend films due to the competing effects of confinement entropy, interaction energy with substrate surfaces, and solidification kinetics. The variations in the vertically segregated composition profile and crystalline order in thin blend films explain the significant impacts of binder polymer choice on the charge carrier mobility of these films in the solution-processed bottom-gate/bottom-contact thin-film transistors.

1. Introduction

Organic thin-film transistors (OTFTs) have recently emerged as a promising low-cost technology for manufacturing flexible, large-area electronics because they provide high field-effect mobility together with the desired solution processability. Recent advances in the molecular design and synthesis of small molecule organic semiconductors have achieved materials with field-effect charge mobilities equal to or exceeding that of amorphous silicon.[1–3] Among small molecule semiconductors, the highest mobilities have typically been demonstrated with single crystals, where the structural defects are minimized.[4,5] Although the electrical performance of single crystal organic semiconductors is excellent, the large-scale fabrication of device circuitry employing single crystals faces enormous processing challenges due to the difficulties of growing uniform crystals and positioning them in a regular manner across a large number of devices.[4] Therefore, current strategies for fabricating large-area organic electronics are focused on solution processing, such as inkjet printing, to achieve thin semiconducting films with high crystallinity and controlled crystal size and orientation.

While solution-coating processes of polymer semiconductors readily result in satisfactory thin films, it is far more challenging to prepare thin uniform films by solution coating of small molecule semiconductors, due to the low viscosity and poor wetting.[6] A promising new approach to improve the solution processability of small molecule semiconductors is the addition of an insulating binder polymer as a thickening and wetting agent.[7–9] This approach has been shown to result in blend films that do not sacrifice the inherent excellent charge mobility of small-molecule semiconductors.[10–13] In blend films, the segregation of the semiconducting small molecules to the gate-dielectric interface is critical to device performance,[14,15] since the charge transport occurs within a very narrow (<10 nm) region adjacent to the dielectric layer; preferential segregation of the insulating binder polymer to the gate dielectric would greatly

Dr. N. Shin, Dr. J. Kang, Prof. D. Y. Yoon
Department of Chemistry
Seoul National University
Seoul, 151-747, Korea
E-mail: dyyoon@snu.ac.kr
Dr. L. J. Richter, Dr. V. M. Prabhu, Dr. R. J. Kline,
Dr. D. A. Fischer, Dr. D. M. DeLongchamp, Dr. S. K. Satija,
Dr. D. J. Gundlach
National Institute of Standards and Technology
Gaithersburg, MD 20899, USA
E-mail: dean.delongchamp@nist.gov
Dr. M. F. Toney
Stanford Synchrotron Radiation Laboratory
Melon Park, CA 94025, USA
Dr. B. Purushothaman, Prof. J. E. Anthony
Department of Chemistry
University of Kentucky
Lexington, KY 40506, USA

DOI: 10.1002/adfm.201201389

decrease the gate capacitance and therefore decrease the transistor current. Moreover, a vertically segregated polymer layer encapsulating the active layer within the blend film can provide enhanced device stability.[10,16,17] Therefore, understanding and controlling the vertical phase-segregation in thin films of small molecule-polymer blends is critical to realizing the blend semiconductors in practical device applications.

Vertical segregation in thin films of small molecule-polymer blends has been identified as important in applications beyond OTFTs. It is very important for bulk heterojunction organic photovoltaic solar cells (OPVs) comprised of polymer donors such as poly(3-hexylthiophene) (P3HT) and small molecule acceptors such as [6,6]-phenyl C61 butyric acid methyl ester (PCBM). This is because segregation of PCBM at the anode and/or segregation of P3HT at the cathode would block the charge transport and degrade the performance of OPVs.[18] Additionally, vertical segregation in polymer-polymer blends has been considered to be important to defining organic light-emitting diode (OLED) characteristics.[19] Despite the critical importance of understanding and controlling the vertical phase-segregation in OTFTs, OPVs, and OLEDs, there have been few systematic studies on the origin of the vertically segregated structure.

Here we investigate the effects of three primary factors that influence vertical segregation in thin films of small organic molecule-polymer blends, i.e., the confinement entropy, the interaction energy with the substrate surfaces, and the solidification kinetics, by employing various insulating polymers blended with the active small molecule semiconductor, 2,8-difluoro-5,11-bis(triethylsilylethynyl)anthradithiophene (diF-TESADT) (**Figure 1**a).[20] We selected atactic poly(α-methylstyrene) (PαMS), atactic poly(methylmethacrylate) (PMMA), and syndiotactic polystyrene (s-PS) as insulating binder polymers. PαMS, previously introduced as the binder polymer in a highly performing blend semiconductor with 6,13–bis(triisopropylsilyl ethynyl) pentacene (TIPS-pentacene),[7,10,12] contains no polar groups. PMMA contains somewhat polar ester groups that interact favorably with and hence typically prefer to wet high surface energy substrates. This favorable interaction energy has been exploited to vary the segregation characteristics of PMMA in P3HT/PMMA blends by manipulating the surface energy of the substrate.[16,21] The comparison of PαMS to PMMA blend provides insight into the influence of the interaction energy with substrates, as compared with the influence of confinement entropy experienced by high molecular-mass polymers at solid interfaces. We also employed s-PS to explore the influence of binder polymer crystallization, because semicrystalline polymer binders, such as isotactic polystyrene (i-PS) and high-density polyethylene (HDPE), have been shown to promote the crystallization and subsequent stratification of organic semiconductors and be beneficial to charge transport properties of devices.[11,22] While s-PS has the same monomer unit as i-PS, the kinetics of its crystallization is much faster than i-PS,[23] leading to fast physical gelation that could inhibit the segregation and crystallization of diF-TESADT. Composition depth profiles of diF-TESADT in blend films were quantified by neutron reflectivity (NR) and variable-angle spectroscopic ellipsometry (VASE). Interface composition and molecular orientation were confirmed by near-edge X-ray absorption fine structure (NEXAFS) spectroscopy. The crystallinity and crystal orientation in the blend films were determined by grazing incidence X-ray diffraction (GIXD). Finally, the electrical performance of bottom-gate/bottom-contact organic thin film transistors prepared by solution processing of various blend semiconductor solutions was found to correlate directly to the vertically segregated composition profile and nanostructure of thin blend semiconducting films.

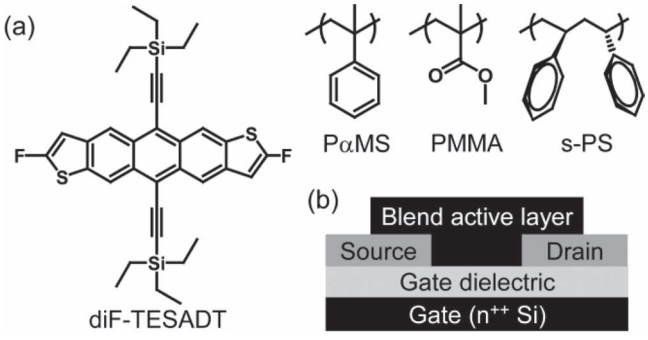

Figure 1. a) Chemical structures of diF-TESADT and various binder polymers employed. b) Schematic structure of bottom gate/bottom contact OTFT device.

2. Results

2.1. Vertical Segregation Profiles by NR

Neutron reflectivity can provide nanometer resolution for composition depth profiles. In this study we use deuterated diF-TESADT to assure adequate contrast between the small molecule and the binder polymer. The reflectivity profile provides quantitative information regarding the total film thickness and any vertically segregated structure, such as the presence of multi-layers, from the appearance of lower and higher frequency Kiessig fringes whose period are inversely proportional to the layer thickness. However, in the presence of broad interfacial widths, the fringes become damped such that modeling the diffuse interfaces is necessary. The primary experimental results for three blend semiconductor films prepared with PαMS, PMMA, and s-PS, respectively, are shown as Fresnel-normalized reflectivity ($R \times Q^4$) in **Figure 2**.

The blend film of diF-TESADT with PαMS exhibits high-contrast, high-frequency Kiessig fringes that provide total film thickness information and indicate low roughness as illustrated by the high amplitude reflectivity fringes for $Q < 0.03$ Å^{-1}. Low-frequency fringes are convoluted with these high-frequency fringes as indicated by the presence of the minimum near $Q = 0.04$ Å^{-1}. This indicates the presence of vertically segregated layers within the total film; in fact only a near symmetric layering, or tri-layer is able to reconcile all the data shown as the solid line. Upon conversion from scattering length density (SLD) to volume fraction profiles, the segregated structure formed nearly pure *d*-diF-TESADT layers with 15.4 nm and 12.2 nm thicknesses at the top and bottom interface, respectively. The middle layer of the PαMS blend film contains a volume fraction of *d*-diF-TESADT of ≈ 0.24.

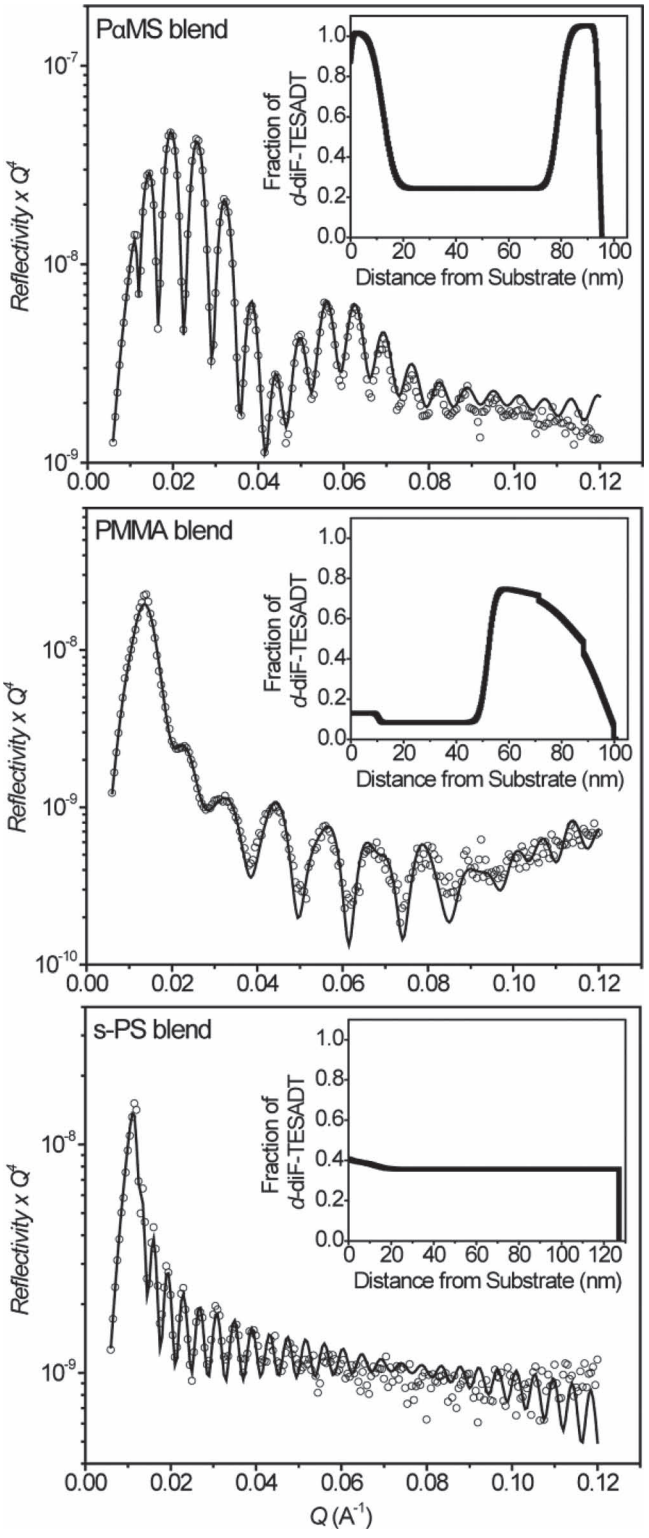

Figure 2. The specular neutron reflectivity ($R \times Q^4$) data for three different blends of polymer with *d*-diF-TESADT. The open circle represents the reflectivity data and the solid line is the best fit based on the corresponding model scattering length density (SLD) profiles, ρ(z). Insets show the volume fraction depth profile of *d*-diF-TESADT in each blend.

The NR result of the diF-TESADT/PMMA blend film, also shown in Figure 2, differs significantly from that of the PαMS blend. The total film thickness appears smaller based on the larger Kiessig fringe period. More importantly, the data indicate a completely different segregation behavior from the PαMS blend, such that a relatively thick and rough *d*-diF-TESADT layer is at the top surface while the majority of the PMMA is located toward the bottom substrate. Due to the predominance of PMMA with less than ≈0.13 volume fraction of *d*-diF-TESADT at the bottom silicon oxide interface, the substrate interface is nearly iso-refractive, providing little SLD contrast. By inspection of the reflectivity maximum between $Q \approx 0.05$ Å^{-1} and 0.08 Å^{-1}, the presence of a weak doublet indicates the presence of a separately stratified thinner layer of highly deuterium-rich material at the top interface. The volume fraction profile converted from the SLD profile ρ(z) revealed that the nearly homogeneous 52.7 nm thick bottom layer is composed primarily of PMMA rather than *d*-diF-TESADT. The 47.8 nm-thick top layer is diF-TESADT-rich, but does not have the SLD ($\rho_{\,d\text{-diF-TESADT}} = 5.10 \times 10^{-6}$ Å^{-2}) of pure diF-TESADT. This is because the PMMA blend film has a very rough film/air interface and the interpretation of the SLD has contributions from a third component, i.e., air. Independent NEXAFS experiments also demonstrate that pure diF-TESADT layer is segregated to the top surface.

The s-PS blend reflectivity is also shown in Figure 2, which shows high-frequency Kiessig fringes without a low-frequency fringe that is the typical signature of vertical segregation. To fit the critical-edge and amplitude, it was necessary to include a 14.7 nm-thick diffuse layer at the silicon substrate that was only lightly enriched with diF-TESADT (having an average SLD (2.89×10^{-6} Å^{-2})). Above that was a uniform blend of average SLD (2.65×10^{-6} Å^{-2}) through the remaining 114.7 nm-thick film. Therefore, the s-PS blend film does not exhibit significant vertical segregation to either interface: the bottom gate dielectric and air.

2.2. Vertical Composition Profiles from VASE

VASE, like NR, can provide insights into vertical segregation. The contrast in VASE, however, arises from the index of refraction (not atomic scattering length in NR) which is a complex function of material composition and structure. This contrast mechanism can enable insights into the molecular order and orientation in the blend film, but also leads to correlations that complicate the data analysis. Shown in **Figure 3** are the normal incidence absorption spectra for diF-TESADT in chloroform solution and in the blend films. Also shown in Figure 3 is the absorption spectrum for a film of neat diF-TESADT, cast from chloroform. The sensitivity of the optical response to local environment is clearly manifested in the absorption spectra. The solution spectra are attributed to isolated molecules. The three features starting at ≈526 nm are a Franck-Condon series (indicating coupling to a vibrational mode of 0.16 eV frequency, characteristic of a C=C stretch) derived from the first singlet transition. Based on Zindo-S calculations[24] we attributed this series to the $A_1 \leftarrow A_1$ transition polarized along the short axis of the conjugated core for the syn isomer. The transition in the anti isomer is predicted to have a similar energy with a transition dipole tipped slightly off the short axis.

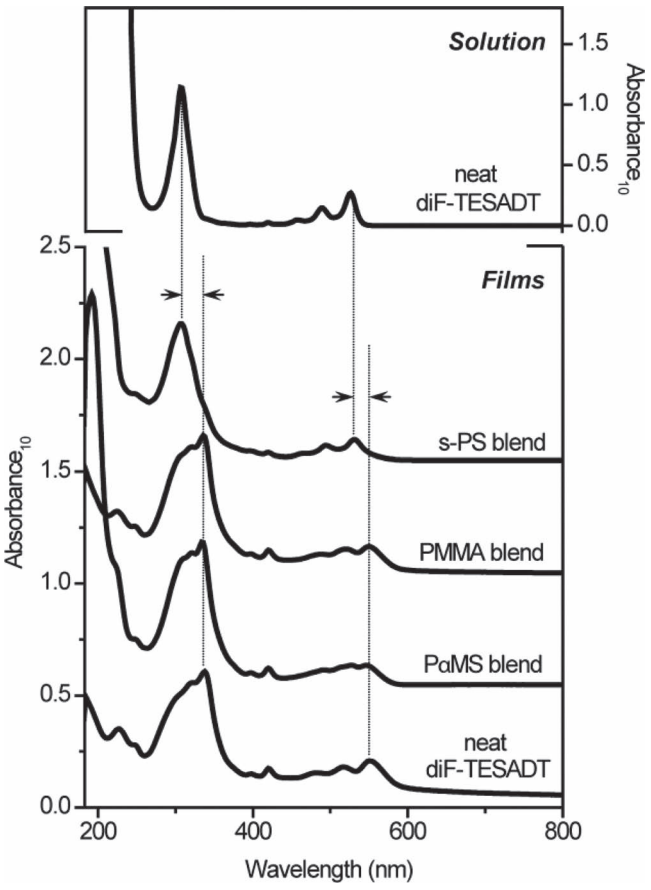

Figure 3. Absorbance from diF-TESADT solution (top), blend films (middle), and neat film (bottom) cast on fused silica. Lines clarify the red-shift attributed to aggregation/crystallization.

The strong feature at 307 nm is attributed to a $B_1 \leftarrow A_1$ transition polarized along the long axis of the conjugated core. Comparison of the solution spectra to that of the neat film establishes a broadening, typical of film inhomogeneities, and red shift of the features, characteristic of aggregation/crystallization. It is known that diF-TESADT crystallizes with a monomolecular unit cell (see below), thus factor-group splittings are not anticipated.

The qualitative aggregation state of the majority of diF-TESADT in the blend films can be directly determined from the absorption data. There is no significant shift in the position of the features in the s-PS blend, indicating that the molecules are in a dispersed, non-aggregated state, consistent with the lack of vertical segregation seen in NR. In contrast, in both the PαMS and PMMA blends, the majority of the diF-TESADT is in an aggregated state, exhibiting the red shifted spectrum. The strong absorbance below 250 nm in the PαMS and s-PS blends is due to the aromatic groups in the binder polymers.

Typical VASE data for the PαMS blend films are shown in **Figure 4**. Motivated by the NR results and the absorption data, the VASE data were fit to a three layer model (top, middle, and bottom). The films were clearly birefringent. Due to the symmetry of spin coating, it was assumed that the films were uniaxial with the major optical axis along the surface normal.

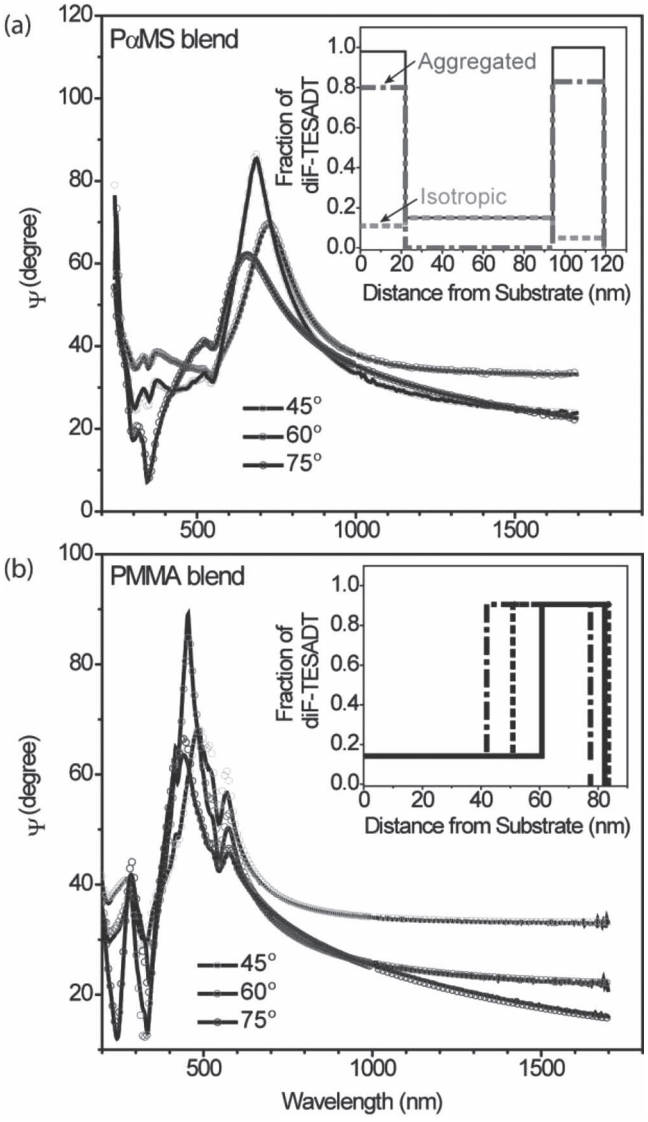

Figure 4. a) Spectroscopy ellipsometry angle Ψ for three angles of incidence (solid line) and model fit (open circle) for data from a PαMS blend film on a native oxide substrate. Inset shows the derived depth profile for diF-TESADT volume fraction (solid line). Also shown is the amount of diF-TESADT in the isotropic dispersed state (gray short dash) and aggregated material with a (001) orientation (gray dash dot). b) Ψ for three angles of incidence (solid line) and model fit (open circle) for data from a PMMA blend film on a native oxide substrate. Inset shows the derived depth profile for diF-TESADT volume fraction from each of the three substrates modeled: native (solid line), thermal (short dash), and fused silica (dash dot).

Each layer was described as a Bruggeman effective-medium mixture of the binder polymer and diF-TESADT. The binder polymer was treated as isotropic with dielectric function determined from neat reference films (see Supporting Information). The diF-TESADT was treated as a linear effective medium mixture of three reference dielectric functions: first one representative of isotropic, dispersed species, determined from fitting the s-PS films, second one representing (001) oriented films, and

third one of mixed, poly-crystalline films (see Supporting Information for details). Figure 4 also shows the model fit to the VASE data, and the extracted spatial profile of the diF-TESADT components. The VASE result is in excellent agreement with the NR, indicating the presence of significant diF-TESADT segregation (1.0 and 0.98 volume fraction) into thin (25 nm and 22 nm) layers at the top and bottom of the film, respectively. The segregated diF-TESADT layers suggested in the VASE model are somewhat thicker than those from the NR model, which may be due to the overall thicker films in the optical series. Due to their distinct spectra, VASE can differentiate between dispersed molecules and aggregates/crystals. Shown in the inset to Figure 4 is the fraction of diF-TESADT in the dispersed state. The model suggests that volume fraction of ≈0.15 diF-TESADT in the middle layer (about 75 nm thick) is entirely in the dispersed state, while the segregated layers are at least 0.95 (top) and 0.88 (bottom) in the aggregated/crystalline state. The total fraction of diF-TESADT in the model fit to the entire film structure is ≈0.48, in nominal agreement with the solution mass fraction.

Also shown in Figure 4 are similar fits to the PMMA blend data. In contrast to the PαMS blend film, the VASE model for the PMMA blend film was not significantly improved by the introduction of a buried interface layer (see Supporting Information), so the results from a bi-layer model (surface layer and bulk) are shown. Overall, VASE data for the PMMA blend cannot be fit with the same fidelity as that of the PαMS. We attribute this to nonidealities in the sample response due to the severe roughness suggested by the NR result. It was necessary to include incoherent patterning of the top layer thickness in the optical model to adequately describe the data. Shown in the inset are the individual depth profiles for the three substrates studied. There is significant variance in the respective film profiles. Nevertheless, the qualitative aspects of the model profile, comprised of a surface layer of nominally 100% diF-TESADT on top of a bulk layer of ≈0.15 diF-TESADT, is again in good agreement with the NR result. As in the PαMS blend case, the surface layer is essentially 100% aggregated/crystalline diF-TESADT. Unlike the PαMS blend, the VASE models suggest that the dilute diF-TESADT in the bulk region is also aggregated/crystalline for the PMMA blend film. There is essentially no dispersed material in the PMMA blend. The average total diF-TESADT fraction of the model fit is 42%.

2.3. Crystallinity and Molecular Orientation by GIXD

Efficient charge transport is intimately related to the molecular orientation and its quality of order in π-stacked arrays, making crystallinity and the molecular packing arrangement two of the most important material parameters for organic electronics device performance. GIXD is a robust tool for measuring the crystalline structure of thin films, providing structural information sensitive to in-plane packing structure (especially near the surface) as well as the out-of-plane packing structures. **Figure 5**a shows the diffraction patterns of the diF-TESADT/polymer blend films along with a neat (binder polymer free) film. Consistent with earlier studies,[25] the neat films are highly crystalline and exhibit at least two primary crystal orientations. Both the PαMS blend and PMMA blend films exhibit strong

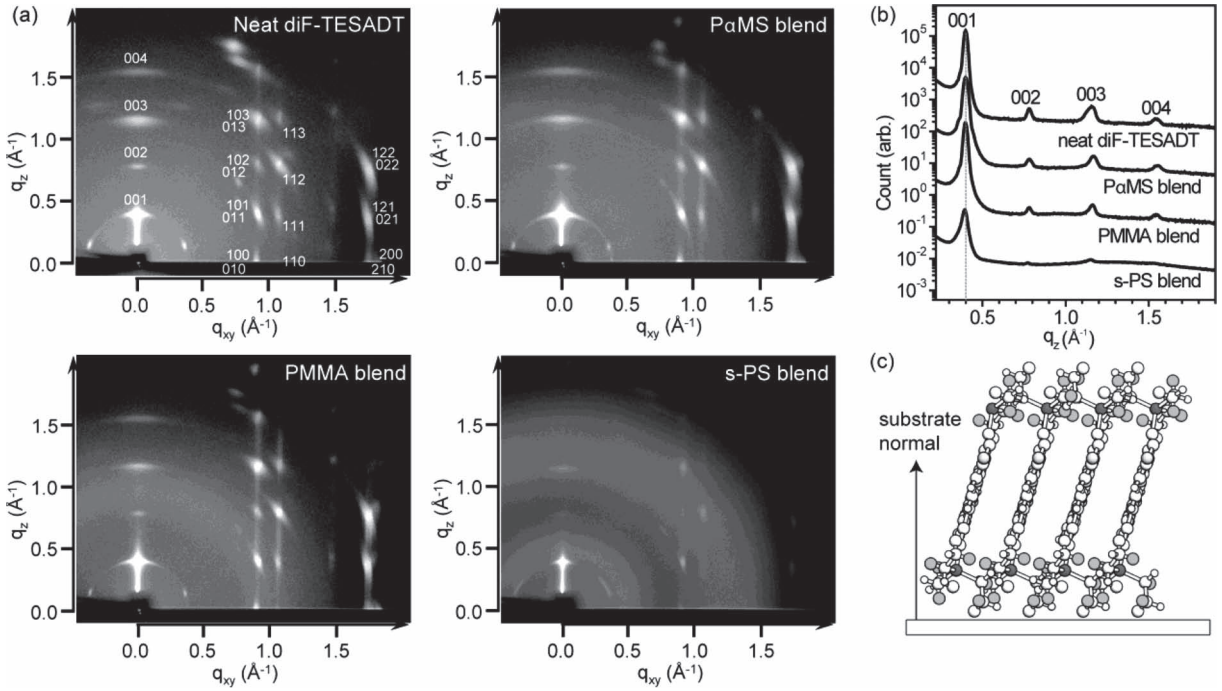

Figure 5. a) 2D GIXD patterns of neat diF-TESADT and blend films with PαMS, PMMA, and s-PS binder polymers on silicon dioxide substrate. b) Vertical scans of the measured X-ray diffraction intensity through the (00*l*) peak series. c) Illustration of *c*-axis oriented diF-TESADT crystal, as viewed along the conjugated plane edge.

diffraction intensity, whereas only a few weak diffraction spots are discernible for s-PS blend film. The weak intensity and the lack of in-plane peaks observed in the s-PS blend is consistent with the absorption spectroscopy, indicating that the bulk of the diF-TESADT exists as a solid solution trapped by the polymer binder. The extent of s-PS crystallinity is expected to be small enough to crosslink, but not extensive enough to create a significant population of highly diffracting crystals.

The PαMS and PMMA blends display nearly identical diffraction peak positions and intensities and similar molecular packing, crystallinity, and crystal orientation. At room temperature, single crystal diF-TESADT has a triclinic structure with unit cell parameters a = 7.21 Å, b = 7.32 Å, c = 16.352 Å, α = 87.72°, β = 89.99°, and γ = 71.94°.[26] The observed peaks in these blend films are consistent with the single crystal structure and do not show evidence for a thin film phase. The (00l) peak series along q_z indicate that diF-TESADT molecules pack in layered stacking relative to the surface normal with d-spacing of 15.8 Å. This d-spacing arises from crystallites with the a–b plane parallel to the substrate. The arc-shape of the (00l) peak series is due to an orientation distribution of a few degrees. The peaks corresponding to in-plane orientations were indexed as the (100), (010), and (110) peaks and are due to packing of the molecular cores. The strong prevalence of these in-plane peaks in the PαMS or PMMA blend films implies that diF-TESADT molecules have a well-arranged π–π stacking structure parallel to the substrate as shown in Figure 5c, which is the desired orientation for efficient charge transport in OTFT devices. The GIXD patterns of the blend films also exhibit the mixed orientation of the crystals on bare SiO_2. The weak (001) features at nominally 20° from the horizon arise from a second distribution of crystals, nominally oriented with the (111) axis along the surface normal. The comparison of the relative intensities of (001) diffraction peaks in rocking-angle scan reveal that the blend films have lower relative population of (111) orientated crystals, which will impede the charge transport in OTFT (Supporting Information).

The full-width-at-half-maximum (FWHM) of the (001) peak from the q_z scan of each sample was obtained by fitting to a Gaussian function and used to estimate the size (T) of diF-TESADT crystals from Scherrer's equation given as $T = 2\pi/FWHM$ in q-space. This analysis estimates the thickness (i.e., z- dimension) of diF-TESADT crystals. The Scherrer formula assumes a well-defined, constant d-spacing and may underestimate the domain size due to the presence of crystal defects. For disordered crystals where d-spacing varies within domains or between domains, the Scherrer's equation is no longer accurate due to the peak broadening from non-uniform strain. The estimated thicknesses of diF-TESADT crystallites (T) are 11 nm and 13 nm for PαMS and PMMA blends, respectively. These dimensions are much thinner than the whole film thickness (≈100 nm), but for the PαMS blends are in good agreement with the thickness of the segregated diF-TESADT layer measured by NR and VASE. The VASE observation of aggregated diF-TESADT at both interfaces would suggest that both regions are highly crystalline.

Polarized optical microscope (POM) images clearly exhibit segregated diF-TESADT crystallites (**Figure 6**). While PαMS and PMMA blend films exhibit a large and interconnected crystalline texture, only isolated small crystallites are observed in the s-PS blend. Spherulite-type crystalline domains which are several tens of micrometers in size are observed primarily in the PMMA blend film, with consequent surface characteristics consistent with the surface roughness complicating VASE modeling of that system.

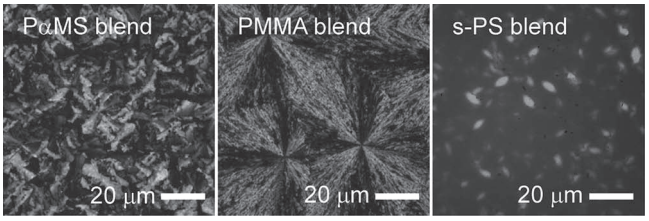

Figure 6. Polarized optical microscope images of diF-TESADT/binder polymer blend films.

2.4. Interfacial Composition by NEXAFS

Carbon K-edge near-edge X-ray absorption fine structure (NEXAFS) spectroscopy is a technique for measuring the composition of organic semiconductor blend films at interfaces.[27] We used NEXAFS spectroscopy to investigate the top and bottom interfaces of the diF-TESADT/polymer blend films. The bottom interfaces were accessed by delamination using a flexible support material attached to the film top.[28] The film composition was determined by fitting the spectra to a linear combination of pure component spectra. If we assume that the electron and photon mean free paths through the both components of the blend are similar, the fit coefficients describe the volume ratio of the two components in the sampled region. In this experiment, we measured the spectra in partial electron yield (PEY) mode, with a grid bias such that ca. 50% of the signal originated within a depth of 4 nm below the sample surface.[29] For the measurements of the bottom interface, we note that this volume correlates closely to the mobile channel region in OTFTs with bottom-gate/bottom-contact configuration;[30] the NEXAFS measurement therefore directly probes the interface which is most significant to the charge transport in the OTFT devices.

NEXAFS spectra are shown in **Figure 7** for the diF-TESADT/PαMS system. The spectra are dominated by the carbon 1s → π^* transitions of the binder polymer and the organic semiconductor. The spectra of diF-TESADT and PαMS are clearly distinct, such that the components can easily be discriminated from one another in the blend. The top-surface spectrum is clearly dominated by the diF-TESADT contribution. A least-squares fit finds the composition to be ≈100% diF-TESADT. A similar analysis was performed on the film bottoms, and also on the other blend systems (Supporting Information), with results shown in **Table 1**.

The NEXAFS results are in excellent agreement with the NR and VASE with respect to the composition of the interfacial layers for the PαMS blend and the composition of the free surface of the PMMA blend. For the bottom interfaces of PMMA blends, the NEXAFS results suggest that there might be very

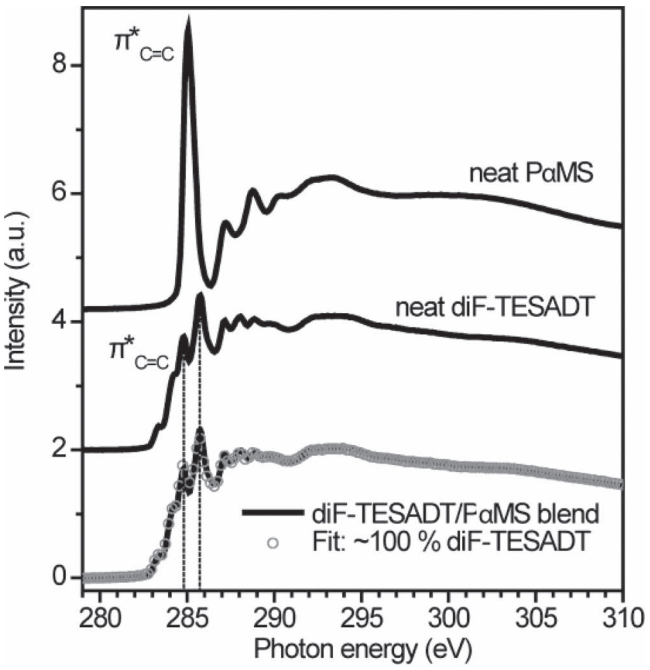

Figure 7. The carbon K-edge NEXAFS data of pure component films and a top film of diF-TESADT/PαMS blend system. The composition of the top interface is found to be ≈100% diF-TESADT. Spectra are offset for clarity. Standard uncertainty in intensity (PEY) is ± 2%; photon energy ± 0.2 eV.

thin buried layers of diF-TESADT, most likely discontinuous, that were not observed by NR and VASE.

2.5. OTFT Device Characterization

We have utilized spin-cast diF-TESADT/polymer blend films as an active layer of OTFTs with bottom-gate/bottom-contact structure as described in Figure 1b. OTFT devices were fabricated without surface modification of dielectric or electrode, corresponding to the clean oxide substrates used in the film characterization studies. **Figure 8**a shows the average saturation mobilities and their standard deviations for the blend semiconductors prepared with PαMS, PMMA and s-PS as the binder polymer, respectively. No significant mobility dependence on channel length was observed for blend films spun on bare dielectric and electrode. Among the three blend systems, the device employing the PαMS blend film exhibited the highest field-effect hole mobility of 0.094 ± 0.042 cm^2/V s and $I_{on}/I_{off} > 10^5$.

Table 1 The volume fraction of diF-TESADT at the interfaces of blend films by NEXAFS

	Fraction of diF-TESADT	
	Top interface	Bottom interface
PαMS blend	1.00	1.00
PMMA blend	1.00	0.52
s-PS blend	0.31	0.10

In remarkable contrast, devices with PMMA and s-PS blend films typically showed very low hole mobility of (1.21 ± 0.53) × 10^{-3} cm^2/V s and (1.75 ± 0.88) × 10^{-4} cm^2/V s, respectively. Moreover, the performance of the PαMS blend film exceeds that of the neat diF-TESADT control film, especially at longer channel lengths (Figure 8a).

3. Discussion

The three binder polymers employed in this work exhibit significantly different behavior with regard to diF-TESADT segregation in thin blend films prepared by solution processing. The vertical phase segregation behaviors in the blend films were shown with consistency by NR, VASE, and NEXAFS. Both of the amorphous polymers, i.e., PαMS and PMMA, exhibit significant vertical stratification, while the crystallizing polymer, s-PS, resulted in a homogenous solid solution.

In PαMS and PMMA blend films, the high level of diF-TESADT crystallization in the amorphous binder polymers, observed from the GIXD and POM, suggests that the large decrease in free energy from crystallization of diF-TESADT is a major driving force for the phase separation upon film formation. In thin films this crystallization-driven phase separation could lead to strong vertical phase segregation under the influence of unbalanced enthalpic and/or entropic driving forces that favor one species over the other at the interfaces.

This mechanism of vertical phase segregation in small molecule–polymer blends is different from that in polymer–polymer blends wherein the biphasic separation in liquid mixtures, due to negligible mixing entropy, drives the vertical segregation as discussed in ref. [19], for example. In this regard, the previous results of TIPS-pentacene and PαMS blend films might demonstrate the dominant role of crystallization in driving the phase separation and vertical phase segregation. As reported in ref. [12], the as-spun blend film of TIPS-pentacene and low molecular-mass PαMS (M_n ≈ 1300 g/mol) showed no clear vertical phase segregation, but exhibited a strong vertical phase segregation upon annealing at 100 °C, well above the glass transition temperature (T_g) of the binder polymer, ca. 70 °C. Recently acquired GIXD patterns of the as-spun and thermally annealed films clearly show that TIPS-pentacene molecules are in amorphous state in the as-spun film and then undergo crystallization upon thermal annealing (Supporting Information). This GIXD result, in conjunction with vertical SLD patterns (Supporting Information) by the NR study, indicates that the crystallization of TIPS-pentacene from its amorphous blend with PαMS is the major driving force for the vertical phase segregation in thin films, not the biphasic separation in liquid mixtures of TIPS-pentacene and PαMS as proposed previously.[31]

The bi-layered vertical stratification in PMMA blends can be understood in terms of the enthalpic vertical segregation driving force, due to the favorable interaction energy of polar PMMA with the polar SiO_2 substrate coupled with the low surface energy diF-TESADT crystal favoring the air surface.

In contrast, the segregation behavior of PαMS blends cannot be explained in terms of interaction energy (enthalpy) alone. Since the polarities of hydrophilic SiO_2 substrate and

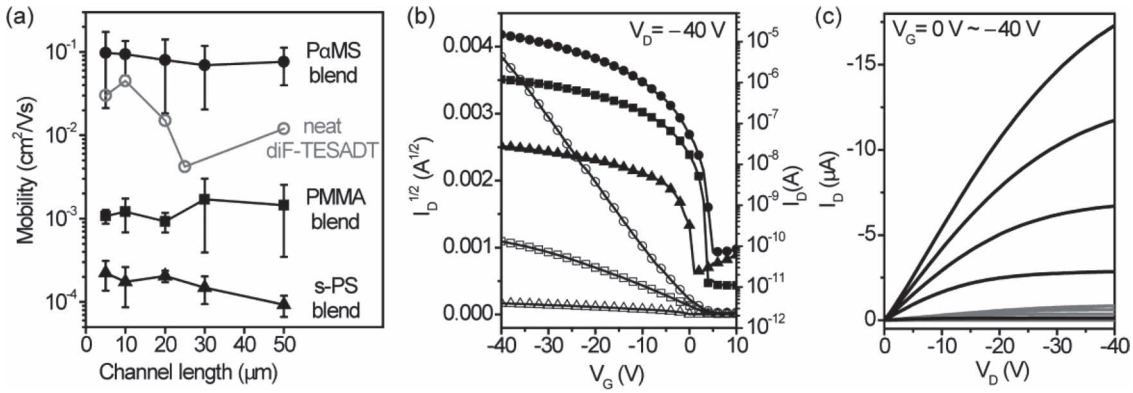

Figure 8. a) Average mobilities of diF-TESADT/polymer blend active layers as a function of channel length. The data points show the average values for eight devices and the error bars represent the standard deviations. The data for neat diF-TESADT are taken from ref. [25]; although no error bars are reported, the offset in values between the average for the PαMS blend and the neat is probably significant. b) The transfer curves of OTFTs for PαMS (●), PMMA (■), and s-PS (▲) blend films, respectively. c) The comparison of output curves of PαMS (black) and PMMA (gray) blend OTFTs at V_G = 0, –10, –20, –30, and –40 V.

hydrophobic air lie at the two extremes, diF-TESADT cannot be preferred by both interfaces in terms of enthalpy. The segregation of diF-TESADT to the air interface is driven by the low surface energy of diF-TESADT, similar to the PMMA blend. In contrast, the segregation of diF-TESADT to the polar substrate is most likely driven by the strong entropy loss of the high molecular-mass PαMS chains confined by the impenetrable solid substrate. Avoiding such an entropy loss would result in the energetically unfavorable diF-TESADT segregation to the SiO_2 substrate. It was shown by theoretical and experimental studies that entropy loss by the confinement of high molecular-mass polymer at the impenetrable interface results in the entropy-driven structure, competing with the enthalpy effect.[32–35] Therefore, it is plausible that PαMS chains tend to remain in the middle portion of the film away from the both interfaces, resulting in the tri-layered film. The confinement entropy loss will certainly depend on the molecular mass of the binder polymer, and its magnitude will decrease as the molecular mass of the polymer decreases. Therefore, the formation of well-defined tri-layer segregation will not be observed when the molecular mass of PαMS is low enough. This was observed by the previous study of blend films of TIPS-pentacence with PαMS of low molecular mass ($M_n \approx 1300$ g/mol).[12]

It is interesting to note that according to VASE results the diF-TESADT in the bulk of PαMS layer (middle layer) is suggested to be in dispersed state (solid solution), whereas in PMMA blend the diF-TESADT in the polymer bulk is suggested to be crystalline. This might be due to kinetically trapped states during the solidification of blend films, caused by higher T_g of PαMS (ca. 170 °C) as compared with PMMA (ca. 100 °C).

Neither segregation nor significant crystallization was observed in s-PS blend film, even though the polarity of s-PS polymer is not expected to differ from PαMS. The rapid solidification of the diF-TESADT/s-PS blend might be attributed to the binder polymer's tendency to crystallize. The characteristics of crystallizable polymers in solution resemble a gelation process from the physically cross-linked network even in the initial stage of very low degree of crystallinity depending on solution conditions.[36–38] During the film deposition process by spin-casting, the diF-TESADT could be kinetically-trapped among the rapidly solidifying s-PS and thus large scale transport and crystallization cannot occur. It appears that such a fast solidification kinetic process originating from the physically cross-linking gelation of s-PS impedes large-scale diffusion of dissolved diF-TESADT allowing only a small fraction of crystalline diF-TESADT. The s-PS blend film, therefore, demonstrates the important effect of solidification kinetics on the phase-segregation behavior of the blend film during the solution-coating process. This kinetic effect will be crucial to optimize for solution-based fabrication of OTFT devices.

We find that the significant variation in OTFT device performance with binder polymer is directly correlated to the observed vertical composition profile and crystalline order. As the blend films were tested with bottom-gate/bottom-contact configuration OTFT devices, the bottom-segregated layer should be responsible for the charge transport. It was shown previously that neat diF-TESADT films spin-coated on SiO_2 substrates comprised of two different orientations of crystals, (001) and (111), that led to low mobility ($\mu \approx 10^{-2}$–10^{-3} cm^2/V s) values and a significant mobility decrease with increased channel length.[25] In comparison, the blend film with PαMS, with the thin crystalline diF-TESADT layer segregated at the bottom gate interface, results in much higher mobilities of $\approx$ 0.09 cm^2/V s, nearly independent of the channel length. The superior electrical performance of the PαMS blend films to those of neat diF-TESADT films is also consistent with the previous results found for TIPS-pentacene/PαMS blend films[12] and TESADT/PαMS blend films[39] as compared with neat TIPS-pentacene film and neat TESADT film, respectively. Previously, the improved electrical characteristics of blend films were attributed mainly to the zone-refinement effect of removing minute amounts of impurities from the critical gate interface.[39] The channel-length independence of higher mobilities seems to suggest additional beneficial factors of morphological effects such as significant decrease of undesirable (111) crystals in the blend films (Supporting Information) and also favorable crystal grain boundaries, for example, but the detailed understanding is beyond the scope of this work. On the other hand, the blend films with PMMA and s-PS exhibit much lower mobilities of 10^{-3}–10^{-4} cm^2/V s, despite the presence of a minor

fraction diF-TEASDT at the bottom surface, indicating that this minor segregation of diF-TESADT is insufficient to form a continuous charge-transporting channel. Although we limited our device characterizations to the bottom-gated OTFTs due to the technological relevance to large-scale integration processes, the vertical phase segregation characteristics delineated by our study are fully consistent with the excellent electrical properties reported by Hamilton et al. for the top-gated OTFT devices with diF-TESADT blends with poly(triarylamine).[13]

4. Conclusions

The vertically phase-segregated structure and the electrical properties of thin blend films of the small-molecule semiconductor, 2,8-difluoro-5,11-bis(triethylsilylethynyl)anthradithiophene (diF-TESADT), with various insulating binder polymers were studied for organic thin film transistor applications. The vertically segregated composition profile and nanostructure in the blend films were characterized by a combination of complementary experimental methods including neutron reflectivity, variable-angle spectroscopic ellipsometry, near edge X-ray absorption fine structure spectroscopy, and grazing incidence X-ray diffraction. We considered three polymer binders: atactic poly(α-methylstyrene), atactic poly(methylmethacrylate), and syndiotactic polystyrene. The blend film with PαMS binder exhibits a tri-layer structure with thin crystalline diF-TESADT layers segregated at both the top (air) and bottom (substrate) interface. The PMMA blend exhibits a bi-layer structure with a crystalline diF-TESADT layer on the air surface on top of a mostly PMMA layer. The blend film with s-PS binder shows a mostly solution-like uniform dispersion of diF-TESADT with only a slight segregation at the bottom surface. Such a large variation of segregation profile and nanostructure is qualitatively consistent with the competing effects of confinement entropy, interaction energy with substrate surfaces, and solidification kinetics. Moreover, the observed variations in the vertically segregated structure provide a logical explanation for the significant impacts of binder polymer choice on the charge carrier mobility of these films in the solution-processed bottom-gate/bottom-contact thin film transistors, ranging from 10^{-3}–10^{-4} cm^2/V s for PMMA and s-PS blends to 0.09 cm^2/V s for PαMS blend. Finally, our results demonstrate that organic electronic thin-film devices which are critically dependent upon the blending of polymers and small molecules, such as OTFTs and OPVs, need to be prepared with careful control and optimization of vertically segregated structures taking into account the three key factors discussed here: confinement entropy, interaction energy with surfaces, and solidification kinetics.

5. Experimental Section

Materials and Film Deposition: diF-TESADT was synthesized as previously reported and deuterium-labeled diF-TEDSADT was synthesized as described in the Supporting Information. The synthesis results in an approximately equal molar mixture of the syn and anti isomers. The atactic poly(α-methylstyrene) (PαMS) (number-average molecular mass (M_n) ≈ 400 000 g/mol) and syndiotactic-polystyrene (s-PS) (M_n ≈ 250 000 g/mol) were purchased from Polymer Source Inc. and atactic poly(methylmethacrylate) (PMMA) (M_n ≈ 190 000 g/mol) was purchased from Aldrich. All binder polymers were used as obtained.[40]

Blend solutions were prepared by dissolving solid powders of diF-TESADT and polymer binder in a 1:1 mass ratio with total 20 mg/mL concentration. Chlorobenzene (CB, b.p. 131 °C) was the solvent for the PαMS and PMMA blends, while 1,1,1,2–tetrachloroethane (TCE, b.p. 130.5 °C) was used for the s-PS blend. Thin films for structural analysis and electrical measurement were prepared by spin coating these solutions at 1000(2π) rad/min (i.e., 1000 rpm). The thin films were prepared on Si wafer cleaned with acetone and isopropanol, followed by a 10 min UV-ozone treatment and deionized water rinse (unless otherwise noted). The blend films containing PαMS or PMMA were cast from room temperature solutions, whereas the s-PS blend film was cast from a warm (≈70 °C) solution since the s-PS solution forms a thermoreversible gel (by physical cross-linking) very quickly at room temperature. Prepared films were placed under vacuum at room temperature for ≈12 h to remove residual solvent.

Structural Characterization Methods: Neutron reflectivity (NR) measurements were performed on the NG-7 horizontal reflectometer at the National Institute of Standards and Technology (NIST) Center for Neutron Research. The reflectivity was normalized by the incident neutron beam intensity and measured as a function of the scattering wave vector (Q) normal to the film, $Q = 4\pi\lambda^{-1} \sin\theta$, where λ is the fixed incident neutron wavelength of 4.75 Å and θ is the specular angle of reflection. Since neutrons interact with the nucleus, contrast arises from the variations in nuclear coherent scattering length density (b/ν), where b/ν quantifies the total scattering length (b) within molecular volume (ν). The atomic scattering length varies from element to element; however, a large coherent scattering length difference occurs between hydrogen ($b_H = -0.374 \times 10^{-12}$ cm) and deuterium ($b_D = 0.667 \times 10^{-12}$ cm) isotopes. Therefore, the neutron reflectivity contrast may be enhanced by deuterium substitution to measure composition profiles. Considering this, blend samples were prepared using deuterium-labeled diF-TESADT (*d*-diF-TESADT) and corresponding hydrogenous binder polymers. The films for NR were prepared on 76 mm diameter and 3 mm thick silicon wafer substrates.

Measurements of thin films were performed with the neutrons incident through air and reflecting off the silicon substrate. Separate experiments were also performed with the neutron beam incident through the backside of the supporting silicon wafer. This approach was used to check for sensitivity of the critical edge to the vertically segregated structure. Our observations were that this geometry did not provide additional information within the Q-range studied and therefore the results are not shown here. The programs from the reflpak suite (http://www.ncnr.nist.gov/reflpak) were used for elements of the data reduction and analysis. The neutron reflectivity data are fit to model reflectivity curves calculated from scattering length density (SLD) ($\rho = \Sigma\, b_i/\nu$) profiles generated using the Parratt algorithm, where the scattering length of each repeat unit is determined by the sum over the atomic scattering lengths b_i within molar volume leading to the absolute scattering length density. In general, this approach uses successive layers of constant SLD with interfaces smeared by a Gaussian function leading to interfacial widths characterized by error functions. These SLD profiles can be directly converted to volume fraction composition profiles with knowledge of the pure-component scattering length densities determined from a separate experiment. Further details regarding neutron reflectivity can be found elsewhere.[41,42] Uncertainties are calculated as the estimated standard deviation from the mean. In the case where the limits are smaller than the plotted symbols, the limits are removed for clarity. Estimation of the total error in the extracted fit parameters (SLD and composition profiles) is difficult. The precision of the fit parameters, determined by the inverse of the curvature matrix is, in general, less than the significant figures reported.[43]

Variable-angle spectroscopic ellipsometry (VASE) data were obtained with an M-2000D series spectroscopic ellipsometer (J. A. Woollam Inc., Lincoln, NE). To reduce parameter correlations in the complex optical models (vertically stratified, uniaxial films), identical films were characterized on multiple substrates:[44] typically a Si wafer with a native

oxide, a Si wafer with a thick (200 to 270) nm thermal oxide and a fused silica plate. Multiple angles of incidence were acquired (45°, 60°, and 75° for Si with native and thermal oxides and 45°, 52.5°, 60°, 67.5° and 75° for fused silica). For measurements on the fused quartz with the beam incident on the film side of the sample the back reflection of the clean side of the substrate was minimized by index matching to a piece of opaque tape (Magic Tape, 3M Corp., Minneapolis, MN). The light incident on the surface was weakly focused to a ≈300 μm diameter spot using focusing optics to reduce the effect of film heterogeneity and, for the measurements with fused quartz substrates, to aid in the isolation of the light reflected from the desired surface. All data sets were then fit simultaneously, which are described in detail elsewhere.[45] As with the NR analysis, the precision of the model fit parameters is high; in general, better than the significant figures reported.

Grazing incidence X-ray Diffraction (GIXD) measurements were carried out on beam line 11-3 at Stanford Synchrotron Research Laboratory (SSRL). A two-dimensional plate detector (MAR-345) with 2300 × 2300 pixels was located at a distance of 400.8 mm from the sample center. GIXD experiments with TIPS-pentacene/PαMS blend film (Figure S7 in Supporting Information) were performed at 4C2 beam line of Pohang Accelerator Laboratory (PAL), Korea, equipped with 4-circle kappa goniometer, and 2D CCD detector (PI-SCX4300-165/2). The incidence angle was chosen in the range of ≈0.06 to 0.08° to optimize the signal-to-background ratio by incidence above the critical angle of the film but below the critical angle of the substrate. The specimens were prepared on 15 mm × 20 mm silicon substrates with a native oxide.

Near-edge X-ray absorption fine structure (NEXAFS) spectroscopy measurements were performed at the NIST/Dow soft X-ray materials characterization facility, beam line U7A at the National Synchrotron Light Source (NSLS) of Brookhaven National Laboratory. Carbon K-edge spectra were collected in partial electron yield (PEY) mode with a grid bias of –50 V. Composition was determined from spectra collected at the magic incidence angle of 54.7°. Spectra fit to a composition ratio were pre-edge normalized via subtraction to make the average intensity in the range of 280 eV to 283 eV zero. The standard uncertainty in PEY is ± 2% and photon energy is ± 0.2 eV.

Electrical Characterization Methods: To fabricate bottom-gate/bottom-contact OTFTs, highly doped silicon wafers were employed as substrate and common gate electrode. A thermally grown ≈265 nm layer of SiO_2 was used as the gate dielectric. Source and drain electrodes were deposited by thermally evaporating a 3 nm-thick Cr adhesion layer followed by a 50 nm thick Au layer and patterned by photolithography and lift-off process with channel lengths of 5, 10, 20, 30, and 50 μm. After careful cleaning of the substrate by 10 min UV-ozone exposure and subsequent water rinse and nitrogen dry, the active layer was spin cast. The electrical characteristics of the OTFTs were measured in ambient air at room temperature using a Keithley 4200-SCS semiconductor parameter analyzer. Field-effect mobilities were extracted in the saturation regime from the slope of the transfer curve of $I_D^{1/2}$ vs. V_G plot.

Supporting Information

Supporting Information is available from the Wiley Online Library or from the author.

Acknowledgements

The authors gratefully acknowledge the financial support from the National Research Foundation of Korea, and the Information Display R&D Center (F0004031-2007-23), one of the 21st Century Frontier R&D Program of Korean Government. This research was also supported by the Chemistry and Molecular Engineering Program of the Brain Korea 21 Project and by Samsung Electronics Co., LTD. GIXD facility at SSRL is operated by Stanford University on behalf of the U.S. Department of Energy, Office of Basic Energy Sciences. GIXD facility at PAL is funded by Korean government and operated by POSTECH. The NIST Center for Neutron Research is funded by the U.S. Department of Commerce.

Received: May 23, 2012
Revised: July 23, 2012
Published online: August 27, 2012

[1] J. E. Anthony, *Chem. Rev.* **2006**, *106*, 5028.
[2] A. R. Murphy, J. M. Fréchet, *J. Chem. Rev.* **2007**, *107*, 1066.
[3] S. Allard, M. Foster, S. Benjamin, H. Thiem, U. Scherf, *Angew. Chem. Int. Ed.* **2008**, *47*, 4070.
[4] A. L. Briseno, S. C. B. Mannsfeld, M. M. Ling, S. Liu, R. J. Tseng, C. Reese, M. E. Roberts, Y. Yang, F. Wudl, Z. Bao, *Nature* **2006**, *444*, 913.
[5] O. D. Jurchescu, S. Subramanian, R. J. Kline, S. D. Hudson, J. E. Anthony, T. N. Jackson, D. J. Gundlach, *Chem. Mater.* **2008**, *20*, 6733.
[6] N. Stingelin-Stutzmann, E. Smits, H. Wondergem, C. Tanase, P. Blom, P. Smith, D. M. de Leeuw, *Nat. Mater.* **2005**, *4*, 601.
[7] B. A. Brown, J. Veres, R. M. Anemian, R. T. Williams, S. D. Ogier, S. W. Leeming, WO 2005/055248 A2, 2005.
[8] J. Smith, R. Hamilton, I. McCulloch, N. Stingelin-Stutzmann, M. Heeney, D. D. C. Bradley, T. D. Anthopoulos, *J. Mater. Chem.* **2010**, *20*, 2562.
[9] J. Smith, R. Hamilton, Y. Qi, A. Kahn, D. D. C. Bradley, M. Heeney, I. McCulloch, T. D. Anthopoulos, *Adv. Funct. Mater.* **2010**, *20*, 2330.
[10] T. Ohe, M. Kuribayashi, R. Yasuda, A. Tsuboi, K. Nomoto, K. Satori, M. Itabashi, J. Kasahara, *Appl. Phys. Lett.* **2008**, *93*, 053303.
[11] M. B. Madec, D. Crouch, G. R. Llorente, T. J. Whittle, M. Geoghegan, S. G. Yeates, *J. Mater. Chem.* **2008**, *18*, 3230.
[12] J. Kang, N. Shin, D. Y. Jang, V. M. Prabhu, D. Y. Yoon, *J. Am. Chem. Soc.* **2008**, *130*, 12273.
[13] R. Hamilton, J. Smith, S. Ogier, M. Heeney, J. E. Anthony, I. McCulloch, J. Veres, D. D. C. Bradley, T. D. Anthopoulos, *Adv. Mater.* **2009**, *21*, 1166.
[14] R. Ruiz, A. Papadimitratos, A. C. Mayer, G. G. Malliaras, *Adv. Mater.* **2005**, *17*, 1795.
[15] F. Dinelli, M. Murgia, P. Levy, M. Cavallini, F. Biscarini, D. M. de Leeuw, *Phys. Rev. Lett.* **2004**, *92*, 116802.
[16] A. C. Arias, F. Endicott, R. A. Street, *Adv. Mater.* **2006**, *18*, 2900.
[17] A. Salleo, A. C. Arias, *Adv. Mater.* **2007**, *19*, 3540.
[18] L.-M. Chen, Z. Hong, G. Li, Y. Yang, *Adv. Mater.* **2009**, *21*, 1434.
[19] A. C. Arias, N. Corcoran, M. Banach, R. H. Friend, J. D. MacKenzie, W. T. S. Huck, *Appl. Phys. Lett.* **2002**, *80*, 1695.
[20] S. Subramanian, S. K. Park, S. R. Parkin, V. Podzorov, T. N. Jackson, J. E. Anthony, *J. Am. Chem. Soc.* **2008**, *130*, 2706.
[21] L. Qiu, J. A. Lim, X. Wang, W. H. Lee, M. Hwang, K. Cho, *Adv. Mater.* **2008**, *20*, 1141.
[22] S. Goffri, C. Müller, N. Stingelin-Stutzmann, D. W. Breiby, C. P. Radano, J. W. Andreasen, R. Thompson, R. A. J. Janssen, M. M. Nielsen, P. Smith, H. Sirringhaus, *Nat. Mater.* **2006**, *5*, 950.
[23] S. Cimmino, E. D. Pace, E. Martuscelli, C. Silvestre, *Polymer* **1991**, *32*, 1080.
[24] M. A. Thompson, *ArgusLab 4.0.1*; Planaria Software LLC, Seattle, WA, **2004** (http://www.arguslab.com).
[25] D. J. Gundlach, J. E. Royer, S. K. Park, S. Subramanian, O. D. Jurchescu, B. H. Hamadani, A. J. Moad, R. J. Kline, L. C. Teague, O. Kirillov, C. A. Richter, J. G. Kushmerick, L. J. Richter, S. R. Parkin, T. N. Jackson, J. E. Anthony, *Nat. Mater.* **2008**, *7*, 216.

[26] O. D. Jurchescu, D. A. Mourey, S. Subramanian, S. R. Parkin, B. M. Vogel, J. E. Anthony, T. N. Jackson, D. J. Gundlach, *Phys. Rev. B* **2009**, *80*, 085201.
[27] D. S. Germack, C. K. Chan, B. H. Hamadani, L. J. Richter, D. A. Fischer, D. J. Gundlach, D. M. DeLongchamp, *Appl. Phys. Lett.* **2009**, *94*, 233303.
[28] A. Salleo, R. J. Kline, D. M. DeLongchamp, M. L. Chabinyc, *Adv. Mater.* **2010**, *22*, 3812.
[29] M. Zharnikov, S. Frey, K. Heister, M. Grunze, *J. Electron. Spectrosc. Relat. Phenom.* **2002**, *124*, 15.
[30] G. Horowitz, *J. Mater. Res.* **2004**, *19*, 1946.
[31] T. Ohe, M. Kuribayashi, A. Tsuboi, K. Satori, M. Itabashi, K. Nomoto, *Appl. Phys. Express* **2009**, *2*, 121502.
[32] T. F. Schaub, G. J. Kellogg, A. M. Mayes, R. Kulasekere, J. F. Ankner, H. Kaiser, *Macromolecules* **1996**, *29*, 3982.
[33] S. K. Kumar, D. Y. Yoon, *Macromolecules* **1989**, *22*, 3458.
[34] A. Hariharan, S. K. Kumar, T. P. Russell, *Macromolecules* **1990**, *23*, 3584.
[35] R. S. Krishnan, M. E. Mackay, P. M. Duxbury, A. Pastor, C. J. Hawker, B. V. Horn, S. Asokan, M. S. Wong, *Nano Lett.* **2007**, *7*, 484.
[36] T. Roels, F. Deberdt, H. Berghmans, *Prog. Colloid Polym. Sci.* **1996**, *102,* 82.
[37] V. Vittoria, F. de Candia, P. Iannelli, A. Immirzi, *Macromol. Chem. Rapid. Commun.* **1988**, *9*, 765.
[38] Y. G. Lin, D. T. Mallin, J. C. W. Chien, H. H. Winter, *Macromolecules* **1991**, *24*, 850.
[39] Y. S. Chung, N. Shin, J. Kang, Y. Jo, V. M. Prabhu, S. K. Satija, R. J. Kline, D. M. DeLongchamp, M. F. Toney, M. A. Loth, B. Purushothaman, J. E. Anthony, D. Y. Yoon, *J. Am. Chem. Soc.* **2011**, *133*, 412.
[40] Certain commercial equipment, instruments, or materials are identified in this paper to foster understanding. Such identification does not imply recommendation or endorsement by the National Institute of Standards and Technology, nor does it imply that the materials or equipment identified are necessarily the best available for this purpose.
[41] T. P. Russell, *Physica B* **1996**, *221*, 267.
[42] T. P. Russell, *Mater. Sci. Rep.* **1990**, *5*, 171.
[43] P. R. Bevington, *Data Reduction and Error Analysis for the Physical Sciences*, McGraw-Hill, New York **1969**.
[44] M. Tammer, A. P. Monkman, *Adv. Mater.* **2002**, *14*, 210.
[45] D. S. Germack, C. K. Chan, R. J. Kline, D. A. Fischer, D. J. Gundlach, M. F. Toney, L. J. Richter, D. M. DeLongchamp, *Macromolecules* **2010**, *43*, 3828.